Supplementary material: Microwave-induced mechanical activation of hydrogel dimers

H.K Khattak,[1] S.R Waitukaitis,[2] and A.D Slepkov[1, a)]

[1)] *Department of Physics & Astronomy, Trent University, Peterborough, ON, Canada K9L 0A6*

[2)] *AMOLF, P.O.Box 41883 1009 DB Amsterdam, The Netherlands*

(Dated: 4 July 2019)

[a)] Corresponding author: aaronslepkov@trentu.ca

I. SPHERE PREPARATION

We used "water beads large" sourced from Water Beads Canada for all experiments. The spheres were hydrated in a solution of $0.5\,\mathrm{g\,L^{-1}}$ KCl and $5\,\mathrm{g\,L^{-1}}$ black Rainbow Dust ProGel dye, as a contrast aid for high-speed imaging. The spheres hydrate to a range of shapes and sizes, but only symmetric spheres with a mass of $(2.8 \pm 0.1)\,\mathrm{g}$ were selected for study. Before each run, the spheres were soaked in a supersaturated NaCl solution, to aid in sphere sparking, which tends to make bouncing more likely. Spheres washed in de-ionized water do not reliably spark, despite forming a hotspot at the point of contact.

II. HOUSEHOLD MICROWAVE OVEN USE

Household microwave ovens have a warm up period of up to a few seconds. A Reed St-2G leakage detector is used to determine when irradiation begins for the device used in this study ($\sim$2 s after start). We also note that these experiments can be damaging to the ovens. Trials in quick secession should be avoided, and the number repeated measurements is limited, before sparking no longer occurs and a replacement oven is required. Although the phenomenon can occur with most commercial microwave ovens, we find Panasonic ovens to be particularly reliable for these experiments. Specifically we used the NN-6D691S model for the majority of the results. The mesh for our imaging port is made from the door of another microwave, with the enamel stripped to ensure an electrical connection between the oven and the window.

III. MICROWAVE PLASMA INTENSITY OSCILLATIONS

It could be presumed that the AC input of the microwave influences bouncing behavior. Analysis of the visual intensity of the plasma reveal a dominant frequency at 120 Hz (the mains driving frequency) which is not in line with the $\sim$15 Hz bounce oscillations. We have also observed many bouncing sequences in the irradiated dimer system where no plasma is recorded. Thus, while formation of a plasma may assist in the seeding of gap oscillations, it is not driving the effect. The vaporization of water or other ejecta at the point of contact is distinct from the plasma itself.

IV. AUDIO SIGNALS

We account for the background audio/interference caused by the operating oven by recording a blank "noise profile" and using software (Audacity) for noise cancellation. Along with the audio spectrum of the spheres, we also captured audio signals of other plasma formations in the microwave to ensure that the audio signals attributed in the main text to gap-oscillations were not from the plasma itself. We find that the signals of plasma are in general a higher frequency and more varied from run to run than that of the spheres (Fig. S1).

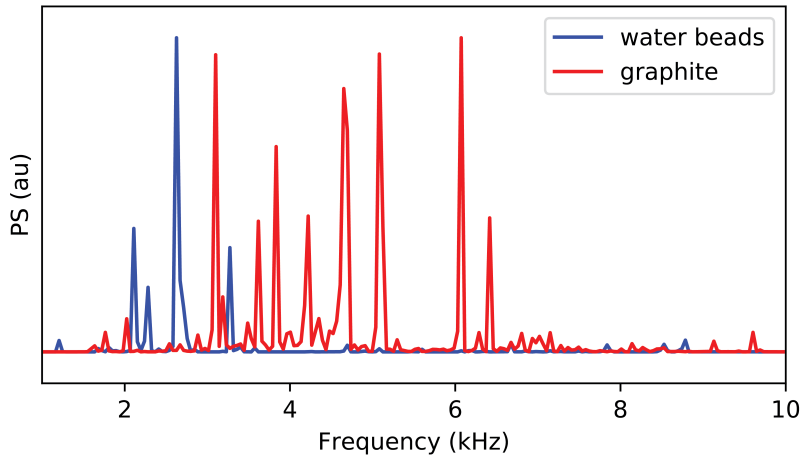

FIG. S1. Power spectra of audio signals for systems under microwave irradiation, filtered by a rectangular window function. The solid blue line is an average signal for water spheres, the red dashed line is an average signal from a graphite rod (mechanical pencil lead), which represents a bulk plasma signal in the absence of mechanical loading.

V. ENERGY LOSSES IN EXPERIMENTS

To calculate energy loss due to collision we use the formulation $E_l = \frac{1}{2}\left(v_{in}^2 - v_{out}^2\right)$, and use a piece-wise linear fit in a 40 ms range around a collision to quantify velocities (Fig. S2). To calculate energy losses due to damping we note that the initial center-of-mass position for a cycle is given by $x = r + A_i$ where A_i is the launch amplitude and r is the sphere radius. This means that the spheres collide when $x = r$. We then use the equation for a damped harmonic oscillator with experimental parameters to get a center-of-mass trajectory for a sphere launch at the bounce amplitude. We then track energy losses from this sphere until $x = r$ to get the estimate of energy lost during the slide towards the collision. This is found to be approximately half of the loss throughout the collision.

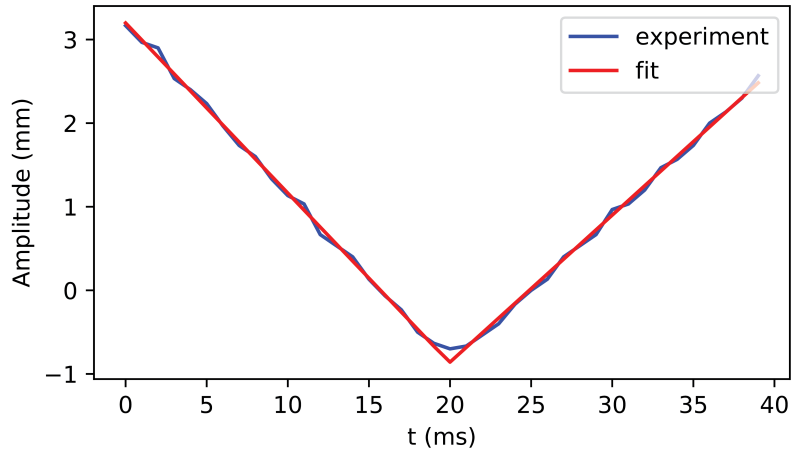

FIG. S2. Plot of bounce amplitude *vs.* time for a collision event for undriven spheres. Included is the actual trajectory as well a peicewise linear fit.

VI. SIMULATIONS

We simulate hydrogel sphere motion according to a procedure adapted from Waitukaitis, *et al.*[1]. Each sphere is modelled as a chain of 301 masses connected by 300 springs. Each mass has a position x_i, and the sum of the spring lengths (each δ) in an unstressed state is set equal to the diameter of the spheres in our experiment (1.8 cm). The sum of the masses is constrained to the total sphere mass (2.8 g). The force between neighboring masses is given by

$$f_i = \kappa \left(\lambda_i - \lambda_i^{-2}\right), \tag{1}$$

where λ_i is the stretch of each spring,

$$\lambda_i = (x_{i+1} - x_i)/\delta. \tag{2}$$

We use this stiffening, non-linear force law to account for the large strains in our system, but also because it prevents springs from passing through each other. We experimentally calculate the average sphere Young's modulus with an Instron 5965 Materials testing apparatus. Empirically, we find that using $\kappa = 0.8$ N produces spring-mass chains with elastic stiffness comparable to the spheres.

The center-of-mass force on the chain (with center-of-mass position and velocity given by x and v, respectively) is given by

$$F = -kx - 2\beta m v, \tag{3}$$

where k and β are taken from experiment ($k = 0.46\,\mathrm{N/m}$ and $\beta = 2.3\,\mathrm{s}^{-1}$). This force is calculated for an entire chain and then distributed evenly across all of the individual masses.

To model the collision between the chains, we turn on a very stiff and highly damped spring that acts on the innermost masses when their separation is less than zero. This force is given by

$$f_s = -k_s x_{sep} - \zeta_s v_{sep}, \tag{4}$$

where x_{sep} is the separation between the innermost masses ($x_{sep} = 2a_s$) and v_{sep} is their relative velocity. This force only turns on if $x_{sep} < 0$. We use values of $\zeta_s = 500$ Nsm^{-1} and $k_s = 10^3\ \kappa/\delta$. The damping parameter is included to suppress spurious contact oscillations and has a negligible effect on the overall dynamics (including the vapor-driven gap oscillations).

Along with the inter-chain collisions, we also model the microwave-induced vaporization and resulting pressure-forces. The vapor exerts a force on each innermost mass given by $F = PA$ where P is pressure and A is the effective contact area. The area is given by

$$A = \frac{\pi}{4}[r^2 - (X_{sep}/2)^2]\theta(2r - X_{sep}), \tag{5}$$

where X_{sep} is the difference in center-of-mass locations of the chains, r is the sphere radius, and θ is the Heaviside function. While modelling the effect of the vapor as a simple force works, explicitly considering it as a pressure acting over an area in the region of contact best approximates the experimental configuration.

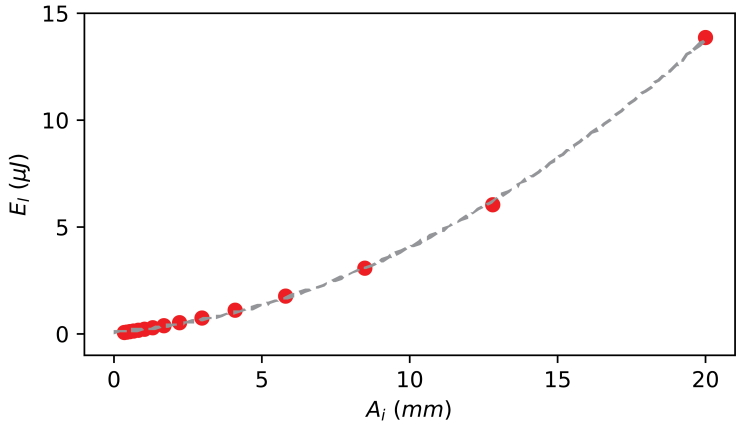

FIG. S3. Plot of energy lost during an undriven collision *vs.* the bounce amplitude for simulated chains colliding along with a parabolic fit of the energy loss.

As in Waitukaitis, *et al.*[1], the pressure evolves as follows:

$$\dot{P} = -P/\tau \text{ until } x_0 \text{ reaches } 0$$
$$\dot{P} = \alpha \text{ until } x_0 \text{ reaches } l^*$$
$$\dot{P} = -P/\tau \text{ until } x_0 \text{ reaches } 0$$
$$\vdots$$

We find that the parameters $\alpha = 5$ GPa s^{-1}, $l^* = 25$ μm and $\tau = 2.5$ μm produce results that match the experimental energy injection and frequency behavior well, with moderate changes in these parameters yielding a relatively small effects on bounce amplitude and frequency. We also note that, compared to the hotplate system of Waitukaitis, *et al.*, the pressure buildup rate in our system should be higher considering we are dealing with conditions in which plasma forms, *i.e.* considerably higher temperatures. Our parameters are consistent with this observation.

To determine multi-collision trajectories, we simulate releasing the chains from a given position and calculate the center-of-mass rebound position after they separate. The rebound position is then used as the input for the simulation of another collision event. This is repeated for several collisions, building a trajectory that can then be compared to experiment. The energy injected during a collision is measured using the difference in total chain energy after a driven collision as compared to an undriven collision released from the same position.

We can also use simulated trajectories with no vaporization to measure the simulate energy losses during collisions, which are caused by excitation of vibrational modes inside the chain (Fig. S3). We find that when dropped from the steady bounce position, each chain loses $\sim$0.2 µJ during such a simulated collision. Despite the simplifications used for the model, these are of the same order of magnitude as what we measure experimentally (see Fig. 2c inset, in main text).

A. Absence of rolling in experiments and model

The possibility of rolling motion has been ignored both in our modelling of the power-sustained bouncing and in the estimates of (experimental) injected mechanical energy. This

arises from our observations that the incredibly small frictional forces in unloaded hydrogel systems result in the nearly-perfect slipping motion of the spheres down the ramp. High-speed videography confirms this. For example, the first part of supplemental movie 4 shows hydrogel sphere collision initiated by motion down the ramp in the absence of microwave irradiation. Pieces of fishing line have been inserted in the spheres as an aid for visual determination of rotational motion. From inspection, the video shows a near complete absence of gravitationally-mediated rotational motion (in the vertical plane). This is quantified by tracking the orientation of the inserted wire to extract the angular velocity, and therefore rotational energy, of the spheres. This analysis shows that that the rotational energy is less than 5% of translational energy for the relevant experimental conditions.

Although not relevant for hydrogel spheres, rolling motion can be significant in other systems. As an example, the second part of Supplemental Video 4 shows the collision dynamics of a hydrogel sphere paired with a similarly-sized grape—the other aqueous spherical object shown to form microwave-induced plasma and to experience power sustained bouncing. In this case, cross-hairs have been drawn on the grape's exterior as a visual aid for rolling. In this video the grape is observed to roll without slipping, while the hydrogel sphere slips without rolling. An analysis of the rotation angle of the marker and linear distance travelled by the grape confirms that the grape is essentially perfectly rolling. In a fully-rolling system, 2/5 of the kinetic energy is rotational, resulting in vastly differing motions compared to the sliding only system. For example, as seen in Supplemental Video 4, the grape arrives at the bottom of ramp after the sliding sphere, and the subsequent set of damped collisions are not symmetric about this nadir. Because such rolling motion will lower the amplitude of power-sustained oscillations for a fixed injection of kinetic energy, rolling motion will need to be considered if this work is to be applied to non-hydrogel systems.

Beyond any motion induced by the ramp, we also show that the balance of forces in the dimer collision itself does not tend to induce rotational motion. Using the chain mass described in the simulation section, the center of mass position of a sphere is recorded. With the center-of-mass acceleration, total force is simply calculated via $F = ma$. The off-axis (torque-inducing) damping force is given by $F = 2\beta m$ where β is an experimental parameter. These two forces are then compared across an entire bounce to note if there is any time where the off-axis force would have a large effect (Fig. S4). Since the off axis forces in these simulations are much smaller than forces that cannot impart angular momentum we can ignore the induction of rolling in the hydrogel system.

Finally, we complete a theoretical treatment of the energies in the system, with experimentally informed parameters. During a collision, the force of contact will be so dominant that we can ignore the other forces. Therefore we consider the system when in the sliding regime. Writing out the forces in Fig. S4 (inset) we have:

$$\text{Force:} \qquad F = -kx - 2\beta m\dot{x} \tag{6}$$

$$\text{Torque:} \qquad \tau = \vec{r} \times \vec{F} = r \cdot (2\beta m\dot{x}) \tag{7}$$

where r is the sphere radius, k is the restoring constant and β is the damping parameter. We can integrate the angular velocity $\dot{\theta}$ over time:

$$\dot{\theta} = \int_0^t \ddot{\theta} dt = \int_0^t \frac{2\beta r m\dot{x}}{I} dt = \frac{2\beta r m x}{I} \left(x(t) - x(0)\right) \tag{8}$$

Using $E_{rot} = \frac{1}{2} I\dot{\theta}^2$ and $I_{sphere} = \frac{2}{5} mr^2$ we find:

$$E_{rot} = 5\beta^2 m \left(x(t) - x(0)\right)^2 \tag{9}$$

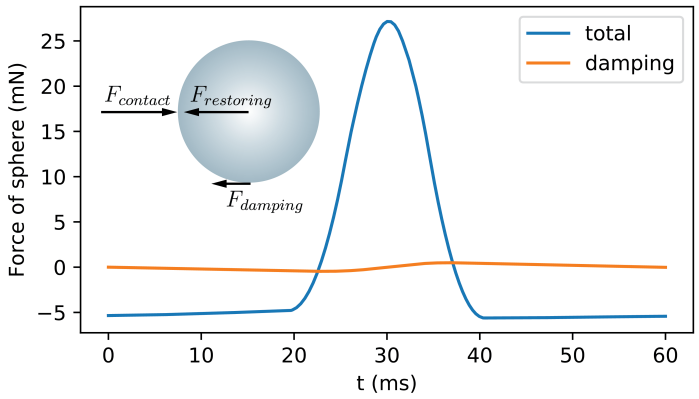

FIG. S4. Plot of smoothed forces as a function of time in a mass chain undergoing a bouncing event, demonstrating that the damping force that could contribute to angular velocity is minimal compared to the total force on the chain. Inset: a diagram indicating the location of the relevant forces on a bouncing sphere

This analysis yileds $\sim 0.2\mu J$, which is below 10% of the total kinetic energy present and well within our experimental uncertainty.

VII. ESTIMATING THE MASS LOSS

We approximate the mass losses due to the vaporization process by assuming ideal gas behavior; $PV = nRT$. The volume we consider is the overlap between two spherical caps, $V_{sc} = \frac{1}{6}\left(3a_s A_h + \pi(a_s)^3\right)$, where A_h is the effective contact area. Based on multiphysics simulations of the electromagnetic hotspot carried out previously[2], we estimate the temperature of the vapor to be ∼700 K. This formulation gives the total mass of vapor trapped between the spheres as during a single oscillation cycle as

$$m_{vap} = \frac{2PV_{sphericalcap}M_W}{RT}, \tag{10}$$

where M_W is the molar mass of water. By assuming all vapor is released after each cycle, we can sum the m_{vap} maxima over the ∼10 oscillations that make up a single collision to estimate the each sphere loses ∼0.8 mg per bounce.

REFERENCES

[1]S. R. Waitukaitis, A. Zuiderwijk, A. Souslov, C. Coulais, and M. van Hecke, Nature Physics (2017), 10.1038/nphys4194.
[2]H. K. Khattak, P. Bianucci, and A. D. Slepkov, Proceedings of the National Academy of Sciences **116**, 4000 (2019).

VIII. SUPPLEMENTARY VIDEOS

Movie 1: Video of hydrogel spheres as they bounce under irradiation in a microwave oven. Recorded using a Nikon D7000 with a 50mm f1.4 lens.

Movie 2: High speed video of hydrogel spheres as they bounce off each other in the track, recorded using a Megaspeed 55K high speed camera.

Movie 3: Animation of simulated aqueous sphere bouncing events in the presence and absence of microwave irradiation.

Movie 4: High speed videos of hydrogel spheres and grapes respectively sliding and rolling down the track in the absence of microwave irradiation. The objects are marked physically to assist in quantification of angular motion.